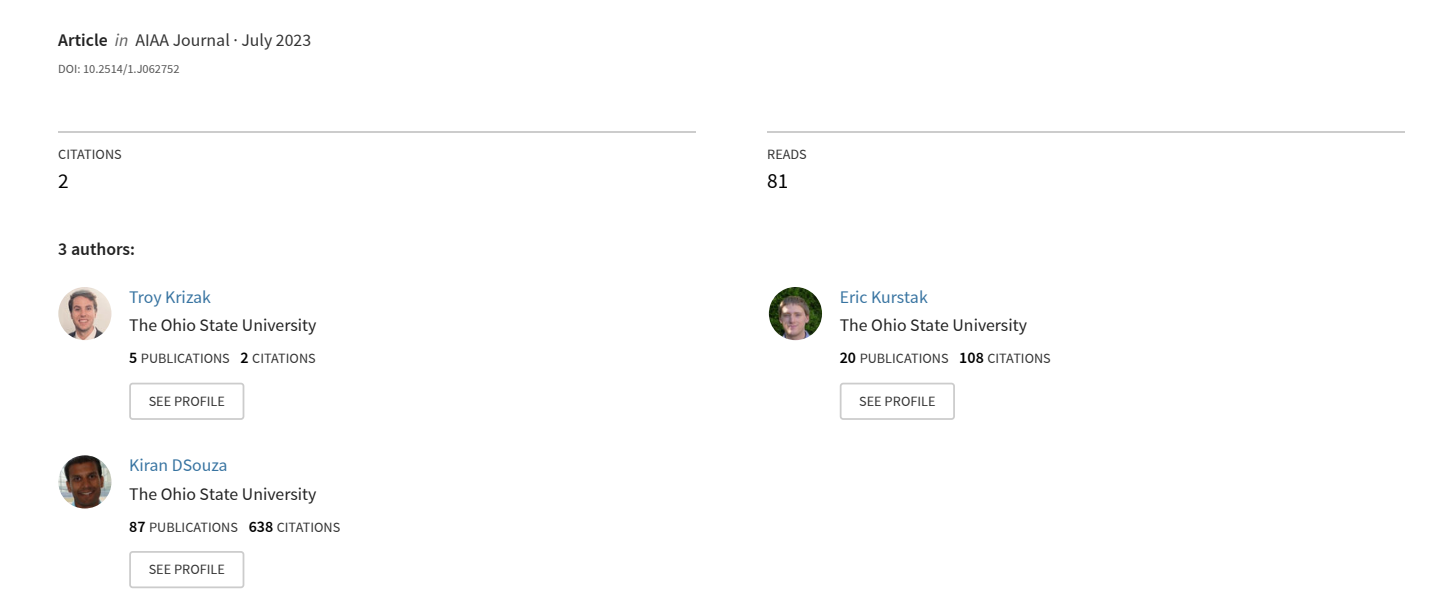
# Experimental and Computational Study of a Rotating Bladed Disk with Under-Platform Dampers



# Experimental and Computational Study of a Rotating Bladed Disk with Under-Platform Dampers

Troy Krizak\*, Eric Kurstak †, and Kiran D'Souza ‡
The Ohio State University, Columbus, Ohio, USA

There has been an extensive amount of work developing reduced order models (ROMs) for bladed disks using single sector models and a cyclic analysis. Several ROMs currently exist to accurately model a bladed disk with under-platform dampers. To better predict the complex nonlinear response of a system with under-platform dampers, this work demonstrates how two linear models can determine bounds for the nonlinear response. The two cases explored are where the under-platform damper is completely stuck and also where the damper slides without friction. This work utilizes the component mode mistuning method to model small mistuning and a parametric reduced order model method to capture changes in properties due to rotational speed effects. Previously, these ROM methodologies have modeled freestanding bladed disk systems. To evaluate the ROM in predicting the bounds, blade tip amplitudes from the models are compared with high-speed rotating experiments conducted in a large, evacuated vacuum tank. The experimental data was collected during testing using strain gauges and laser blade tip timing probes. The blade amplitudes of the tip timing data, strain gauge data, and computational simulations are compared to determine the effectiveness of the simplified linear analysis in bounding the nonlinear response of the physical system.

### I. Introduction

Researching dynamic and vibratory properties of bladed disks in gas turbines is essential when designing turbomachinery to become more efficient and reliable. Two key areas of research are mistuning, which is the result of blade to blade differences breaking the cyclic symmetry of the bladed disk, and damping systems. Damping elements such as under-platform dampers can help mitigate vibration and fatigue problems within bladed disks by using friction to reduce vibration energy, which reduces blade deflection during operation. Proper modeling and analysis of mistuning and damping elements can be used to plan for and mitigate high cycle fatigue (HCF) within bladed disks. HCF results

<sup>\*</sup>Graduate Student, Department of Mechanical and Aerospace Engineering, The Ohio State University, Columbus, Ohio, USA; krizak.1@osu.edu. (Corresponding Author)

<sup>&</sup>lt;sup>†</sup>Postdoctoral Researcher, Department of Mechanical and Aerospace Engineering, The Ohio State University, Columbus, Ohio, USA; kurstak.1@osu.edu.

<sup>&</sup>lt;sup>‡</sup>Associate Professor, Department of Mechanical and Aerospace Engineering, The Ohio State University, Columbus, Ohio, USA, ; dsouza.60@osu.edu. AIAA Associate Fellow

from the high frequency, low amplitude response of blades that operate over many hours and leads to millions of cycles and is therefore a large source of high cost failures and mishaps within the gas turbine industry. Full finite element (FE) models have been constructed to analyze the vibrations present in bladed disks for many different scenarios. Using full order models for vibratory analysis is only viable for academic models and is not realistic for current industrial models that have complex geometries and require large degree of freedom models to accurately represent their full dynamics. Fundamentally, these systems are very complex high dimension nominally cyclic systems with mistuning, varying contact states, and friction at the interface between the damper and under-platform region of the bladed disk. This work is important because it shows how specific simplified models can capture some of the extremes in the contact conditions to give estimates in the expected ranges of motion for these complex systems.

A key requirement for ROMs of bladed disks, due to the size of these systems, is that they are generated from single sector models using cyclic analysis calculations. For small frequency mistuning, the first set of powerful ROMs that were developed in this manner and could be as small as the number of sectors in the bladed disk are Fundamental Mode of Mistuning (FMM)[1] and Component Mode Mistuning (CMM)[2, 3]. FMM is limited to single isolated blade dominated mode families, while CMM is more flexible and can handle multiple mode families and all types of modes if the model is large enough. After these models were developed, a number of other methods have been developed to handle a variety of other types of mistuning including small geometric mistuning[4–6] and a tool for almost any type of large or geometric mistuning[7]. Additionally, the challenge of multiple stages with different number of sectors combined with small mistuning[8, 9], large mistuning[10, 11], and aero elastic effects[12] has also been addressed.

Extending these effective ROMs to nonlinear systems has always been a challenge. However, there are techniques that have been developed to reduce the bulk of the linear degrees of freedom of the system while keeping the more localized nonlinear degrees of freedom active. These methods often use the harmonic balance method[13] to effectively model the nonlinear system. These nonlinear ROMs have been used to model friction damping when there are under-platform dampers[14] and ring dampers[15, 16] applied to the bladed disk and blisks, respectively. Recently, there has also been work in modeling cracks for bladed disks using analysis of the system when it is operating in its linear states[17, 18]. Constructing a ROM that can handle these nonlinear systems is very valuable and is a continued point of research in the turbomachinery industry.

Validating these new linear and nonlinear ROMs with actual experimental data is a challenge due to the nature of the systems, primarily the testing needs to be conducted at rotational speeds experienced during operation. The rotating experiments ensure the proper stress state in the bladed disk and the proper boundary conditions between the blade dovetail or fir tree and the disk slot as well as between the damping elements and the blade or disk. This work uses experimental data from high speed rotating experiments conducted at The Ohio State University (OSU) Gas Turbine Laboratory (GTL) in a facility designed for damping and mistuning studies[19] and has previously been used to study synchronous[20] and asynchronous vibrations[21] for linear undamped bladed disks. This work seeks to analyze data

from these nonlinearly damped experiments and relate it to linear computational parametric reduced order models (PROMs) developed to handle the mistuning at speed[22]. Moreover, this work will also discuss the effectiveness of relating tip timing data to strain gauge information using the appropriate computational models. Strain gauges are well established but rely on slip rings, are costly to install, and interfere with the dynamic properties of the system. An alternative, noncontact, measurement technique such as laser tip timing is preferred. A primary strength of blade tip timing is the ability to measure blade tip displacements of all the blades in a stage without having to apply strain gauges to each blade.

The remainder of the paper is structured as follows. First, an overview of the experiments is provided, which will include a brief description of the facility and measurement systems. Next, the computational methodology will be described, including a review of the PROM with small mistuning, a discussion of the damper modeling, and how the computational and experimental measurements are compared. After that, results for both linear freestanding and nonlinear damped blade models are discussed with a comparison to strain gauge and tip timing experimental results. Finally, conclusions about the results of the study are presented.

# **II. Experimental Overview**

The following section will discuss the experimental facility and measurement systems used to obtain the experimental data. This data is vital for comparisons and validation of the computational results described in this work. The basic experimental setup consists of first pumping down and evacuating the large spin tank facility (LSTF) using 3 large vacuum pumps that run continuously during the experiment. A single stage bladed disk is then driven quickly by an electric motor to a speed a few hundred revolutions per minute below the mode of interest. The appropriate number of air jets for the given engine order excitation are then turned on as the rotor is accelerated through the critical speeds that causes a synchronous resonance response, here each blade will resonate at a unique rotational speed due to the mistuning in the bladed disk. This process is also repeated as the blades are decelerated through the critical speeds. Additionally, the process is repeated for different acceleration rates through the critical speeds and for different air jet pressures (which correspond to different forcing levels on the blades). The results were repeatable, and response of the bladed disk varied linearly with forcing amplitude for the freestanding case. The primary focus of the experimental studies was to measure tip deflections during resonance. The data acquisition for the strain gauges are turned on and off during the excitation through each ramp through a critical speed. The light probe system is initialized, and probes are checked to make sure they are operating effectively when the system reaches a few thousand revolutions per minute and then can start acquiring measurements through several data runs. This is because the data is under sampled compared to the strain gauges. The light probes also allow for real time monitoring of the blades to ensure that the tip deflections do not get too large.

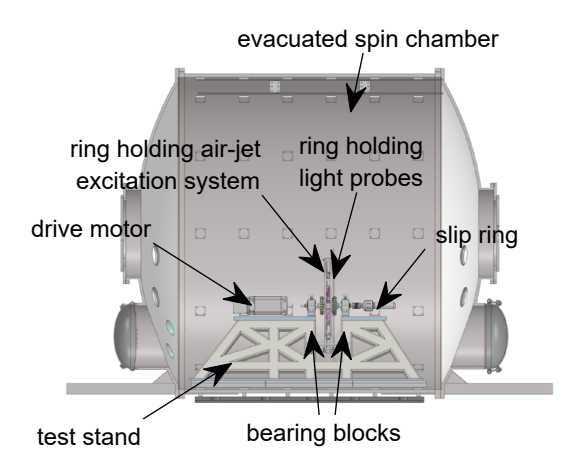


Fig. 1 Experimental test rig in above ground spin tank

#### **Facility**

The OSU GTL has developed an above ground LSTF that is designed to study the structural dynamic response of rotating machinery at design speed while in a vacuum[19]. The large volume tank and use of multiple large vacuum pumps make it useful for studying damping and mistuning because non-contacting forcing mechanisms, such as air jets, can be used. This retains the original system dynamical properties. A schematic of the current test configuration, with key components highlighted, can be seen in Fig. 1. A test stand is bolted to the floor of the spin tank facility, and all key testing components including the drive motor, bearings, rotor, slip ring, excitation system, and tip timing system are mounted to the test stand.

An air jet excitation system was used to force the system, while accelerating through critical speeds, to excite blade resonances for the first bending mode. Air jets are preferred over other excitation systems because they are non-contact, work well in a vacuum, and do not interfere with the laser light probes. The most beneficial characteristic is that the air jets are non-contact, so they do not alter the blade dynamic properties as an electromagnetic or piezoelectric system would. The air jets have the ability to excite both synchronous[20] and asynchronous[21] vibrations, but synchronous vibrations will be the focus of this work. Synchronous vibrations are expected excitations and can be predicted using a Campbell diagram, whereas asynchronous vibrations are due to aerodynamic instabilities such as vortex shedding and cannot be predicted from a structural analysis. Synchronous vibrations were generated by placing the air jets evenly around the perimeter to excite the given engine order (EO) and letting air flow through the jets as the rotor was accelerated through a critical speed. A mounting ring was used to accurately place the air jets evenly around the perimeter of the bladed disk. The bracket that holds the air nozzles can be placed to the precision of 0.2 degrees. Nozzles were set near the blade tips at the midchord to excite the first bending mode family. The air jets are all connected to the same air supply and have the same nozzles and valves, so that all jets supply the same mass flow. During the testing,

different levels of pressures were used to vary the forcing magnitude on the bladed disk. For synchronous vibrations, the forcing frequency is dependent on the rotational speed and the engine order. The equation for forcing frequency can be seen in Eq. (1), where EO is the engine order of excitation and  $\Omega_{rotor}$  is the rotational speed.

$$f_{mode} = EO * \Omega_{rotor} \tag{1}$$

A specific EO is excited by turning on the corresponding number of air jets. For example, an engine order four excitation has four evenly spaced air jets turned on. The placements of the air jets with examples of EO forcing can be seen in Fig. 2, with the filled circles representing air jets that are turned on for each engine order.



Fig. 2 EO4, EO5, and EO6 forcing with air jets

There are several drive systems available for the LSTF that can be used to accelerate the bladed disks to the desired operating speeds. These include air motors, a hybrid electric motor, and an electric motor. The electric motor was utilized in this testing to better control the acceleration and deceleration through the expected resonant crossings. The electric motor was used to accelerate and decelerate the rotor at rates of 7 RPM/s and 15 RPM/s.

The described experimental facility has the ability to measure two types of real-time data, health measurements of various components and dynamic response data of the bladed disk. The health measurements include pressure, temperature, and accelerometer information of different components in the tank, particularly the bearings. The real time dynamic measurements are captured with an eight probe Agilis Measurement Systems that computes all blade tip deflections in real time. Additionally, dynamic measurements of the blades were taken with strain gauges attached to the blades. These strain gauge signals were conditioned and amplified before sending them through a slip ring and recorded on the stationary high speed data acquisition system. These strain gauge measurements were available for offline analysis after each test was completed. Both the strain gauge and tip timing measurement methods will be expanded upon in the next sections.

In this work two cases will be explored, namely the linear freestanding blades case and the nonlinear case with under-platform dampers installed. When under-platform dampers are present, the blade dynamics are expected to change by increasing the natural frequencies of the blades and decreasing the blade tip deflection amplitude for a given forcing level. This change in natural frequency can be seen in Fig. 3 where it is shown that the normalized natural frequencies

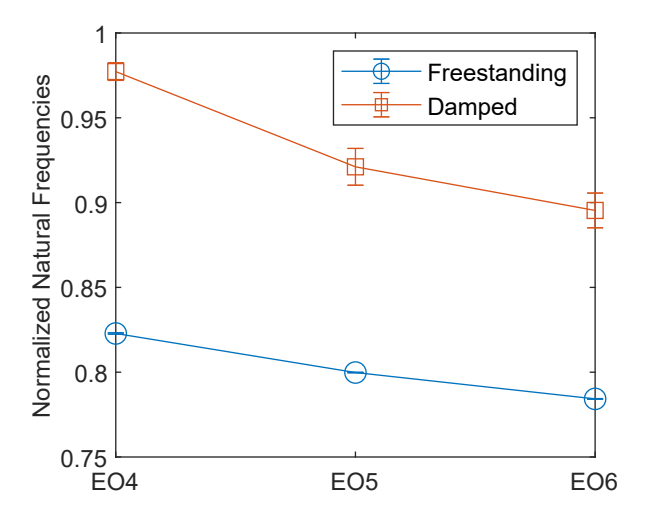


Fig. 3 Natural frequencies for different engine orders for damped and undamped blades

for the damped cases are much higher than that for the freestanding case. The average values and standard deviations for the EOs are extracted from the different levels of forcing runs. It can also be seen that for both the damped and the freestanding cases, the natural frequencies decrease as the engine order number increases. This is because the different EOs have different rotational speeds, a higher rotational speed will result in an increased stiffness. Lastly, it can be seen that the damper cases have more variation in the natural frequencies from the different forcing cases, this is because the state of the damper changes with different levels of forcing. This will change the mode shapes of the blades and the overall stiffness of the system, which leads to more variability in the natural frequencies. This is elaborated upon in the results section of the paper. The addition of a nonlinear damping element also presents a challenge for creating an accurate computational model. A study was previously performed at the OSU GTL to demonstrate the impact of adding these damping elements to the bladed disk [19]. This analysis was repeated for this round of experiments and a key result is shown in Fig. 4, where it is clear that the damper significantly lowers both the average and deviation in the response of the bladed disk. The forcing levels of the freestanding case needed to be cut off when the blades reached amplitudes that could create high cycle fatigue concerns. The damper case could withstand the maximum forcing output that could be delivered with the current rig setup. The results show the average of all the blades over a number of cases of varying acceleration rates and directions for an EO 5 excitation, with the error bars denoting one standard deviation in the response. This is to be expected as the friction damping elements will take energy out of the blades and reduce the blade tip deflection regardless of forcing amplitude. The repeatability in these experiments has been presented in previous work [19].

# **Strain Gauge Measurements**

One type of dynamic data measured during the experiments was from strain gauges physically adhered to key locations on the blades. Strain gauges are a widely used method of measuring responses in the turbomachinery industry

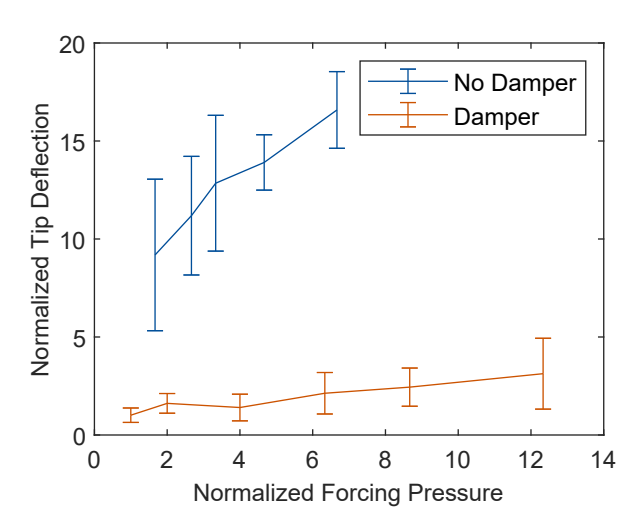


Fig. 4 Blade tip deflections for damped and undamped blades over a number of cases for EO5 excitation

with well-known uncertainties and complications. These strain gauges output a voltage based on the relative deformation at each end of the gauge, which can then be converted into a strain. The signals from the strain gauges are wired to an on-board signal conditioner and amplifier to increase the output signal before it passes through the slip ring. This conditioning and amplification are essential due to the noise added by transmitting the signal through the slip ring. It is important to note that when strain gauges are applied to blades, a minimum amount of adhesive should be used on the gauges and wiring to retain the dynamic properties of the blade.

Four blades were of primary interest in this study and were instrumented with several strain gauges. The blades were chosen based on their mistuning values measured in previous studies; one blade has high mistuning, one has low mistuning, and two have average mistuning. Additionally, every other blade had a strain gauge attached to the root. The four blades of interest were wired with 5 gauges placed at various locations on the blade as well as the root strain gauge. This work will focus on the comparison of tip timing data, ROM results, and the response of a single blade where strain gauges were applied. After the voltage signals are sent to the high-speed data acquisition system, they are converted from the measured voltages into micro-strain using calibration files for the manufactured strain gauges.

A filter was then used on the computed strain signals to remove the high frequency noise from the data. A band-pass fast Fourier transform filter range was selected using a spectrogram to visualize the dominant frequencies present. The filter applied to a single representative strain gauge signal from a single test can be seen in Fig. 5. The top graph in the figure shows the full response of the blade strain as it is ramped through a resonant crossing for both the filtered and unfiltered responses. The bottom graph shows the same signal zoomed in (black box in top graph) to better see the elimination of the high frequency noise.

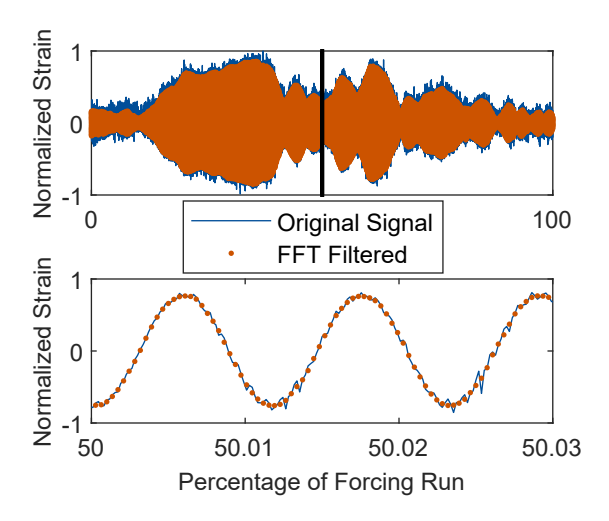


Fig. 5 Band pass filter used to eliminate noise from strain gauge measurements

## **Tip Timing Measurements**

The other type of dynamic data taken during the experiments was blade tip timing data using optical laser light probes. There has been a great deal of work done in measurement systems that provide blade time of arrival data because this data can be processed in real time to monitor all the blade deflections and is a non-contact measurement technique[23-28]. Since tip timing is a newer measurement method compared to traditional methods such as strain gauges, a novelty in this study is the comparison of tip timing with more traditional measurement methods and modeling techniques for a realistic rotor. The particular tip timing system used for the testing in this study was an 8-probe measurement system from Agilis Measurement Systems. Additional information on the measurement system can be found on the Agilis website. Optimization of probe placement was performed that allowed all interested engine orders to be captured accurately. Similar to the air jets, blade tip timing is non-contact, so blade dynamics are kept intact during the testing which is important for these dynamic tests. Since the strain gauges are physically adhered to the blades, they have an impact on the dynamic characteristics of the bladed disks. One key drawback to tip timing systems is that the data is under-sampled; each blade passage produces a single data point per measurement probe, in contrast, strain gauges can continuously taking many samples during one revolution. Reconstructing each blade tip amplitude is dependent on specific algorithms. Without blade vibration, the time of arrival for a blade is dependent solely on the rotational speed. However, when the blade is vibrating blade arrival times are dependent on both the amplitude and frequency of the vibration. After arrival times are measured, blade deflections can be calculated based on the expected arrival time for the specific rotational speed. For this work, measurements were taken near the leading edge to gain sensitivity to the motion of the first bending mode of the blade.

In the LSTF, the tip timing light probes were placed on the same mounting ring as the air jet excitation system to enable easy movement of the probes circumferentially, axially, and radially to measure the appropriate mode family. This also allows for changing where the point of deflection is being measured on the blade tip. The mounting ring allows tip timing probes to be placed within a 0.2 degree tolerance. The Agilis c360 software enabled real time tip deflection measurements, real time blade deflection plots, and Campbell diagrams. The laser tip timing data was also filtered using a similar band-pass technique as the strain gauges, and this was done within the Agilis measurement software. These filtering methods for strain gauges and laser tip timing were applied for both the free-standing and under-platform damped bladed disk cases.

#### **Tip Timing and Strain Gauge Comparison**

In order to compare the strain gauge measurements to the ROM and tip timing results, an accurate FE model needs to be utilized to transform the measured strains into tip deflections. The same industrial FE model used to construct the ROM was used for this correlation. Strain gauge elements were added to the FE model in the same locations as the gauges on the physical blades that were tested. It is important to note that the strain gauge elements must have low mass and stiffness so as to not affect the mode shapes. A pre-stressed modal analysis at the same rotational speed as the strain measurements was then computed. Individual coordinate systems were added for each of the strain gauge elements and were aligned according to how the physical gauges were installed on the blade. The strains from the computational modal analysis were then compared to the tip deflection in the computational analysis to obtain a computational ratio that relates the strain measurements to blade tip deflection. This ratio was then used to convert strain measurements to blade deflections to compare the strain gauge measurements to the tip timing responses in the experiments.

This method for converting strain measurements to tip deflection was applied for both the freestanding and the damped cases, with the computational model being adjusted to either include or not include the damper. Also, because the physical damper is nonlinear, neither of the linear FE model cases alone can be used for this correlation. Therefore, to model these blade deflections, both the stuck damper and the sliding damper models were solved with the strain gauge elements and the average of the tip deflections between the two were used for the correlation.

After the strain data was converted to tip deflection, comparisons were done to determine the validity of the strain-deflection conversion and to assess the overall quality of the agreement between the computational results and experimental data. These comparisons include looking at the max tip deflection and determining if the strain gauges and tip timing show similar blade vibrational amplitudes. It is also important to ensure that these max tip deflections are occurring at the same frequency. Both the tip timing and the strain gauge data are compared to the ROM tip deflection and can be seen in the results section of this work.

#### III. Computational Model

In this section, the methodology that was used to construct the ROM utilizing both the PROM and CMM methods will be described. As mentioned, an industrial bladed disk model was utilized to extract the mass, stiffness, and mode

shapes of the system using a prestressed modal analysis. A standard cyclic symmetry analysis was conducted in ANSYS using a single sector model to compute mode shapes and frequencies of the full bladed disk and the cantilever blade models. This process was also repeated at different prestress levels in order to construct the parametric reduced order model as detailed by Kurstak and D'Souza [11]. The modulus of the initial FE model had to be adjusted slightly to match the average frequency of the mistuned physical system measured in the experiments before these quantities could be used in the PROM-CMM method [11]. Experimental measurements of the zero mean mistuning pattern were added directly to the ROM only using the PROM-CMM method in the reduced space. These extracted values are then used for building the following ROMs. Note that the exact properties of the industrial finite element model cannot be shown, but a simple general bladed disk model can be seen in Fig. 6. The full stage model can be seen in Fig. 6a (note that this full stage model is never constructed for the industrial model since it is too large and only a sector model is used) and the single sector can be seen in Fig. 6b. The single sector model shows the definitions for the cyclic faces, the surfaces that are fixed, and the forcing nodes that are swept across during the time integration. There are approximately 2 million degrees of freedom in a single sector of the industrial model used in this study, which is not unusual for industrial models. A single sector and cyclic analysis were utilized due to the computational size. The rotor model was held fixed on sections of the outer portion of the disk to simulate where the disk was clamped during the testing. To ensure that the computational models are accurate, the material stiffness properties of the blade was tuned to match that of the experiments. The mistuning pattern that was measured in the experiments were implemented in the CMM-PROM method that will be outlined. As discussed, strain gauge elements were added to the finite element model for the conversions of the strain to tip deflections. Approximate gauge locations, on the general blades, can be seen in Fig. 7. There are 5 gauges applied to the blade and 1 applied to the root of the blade that is not shown. The leading edge (LE) and trailing edge (TE) are labeled in the figure.

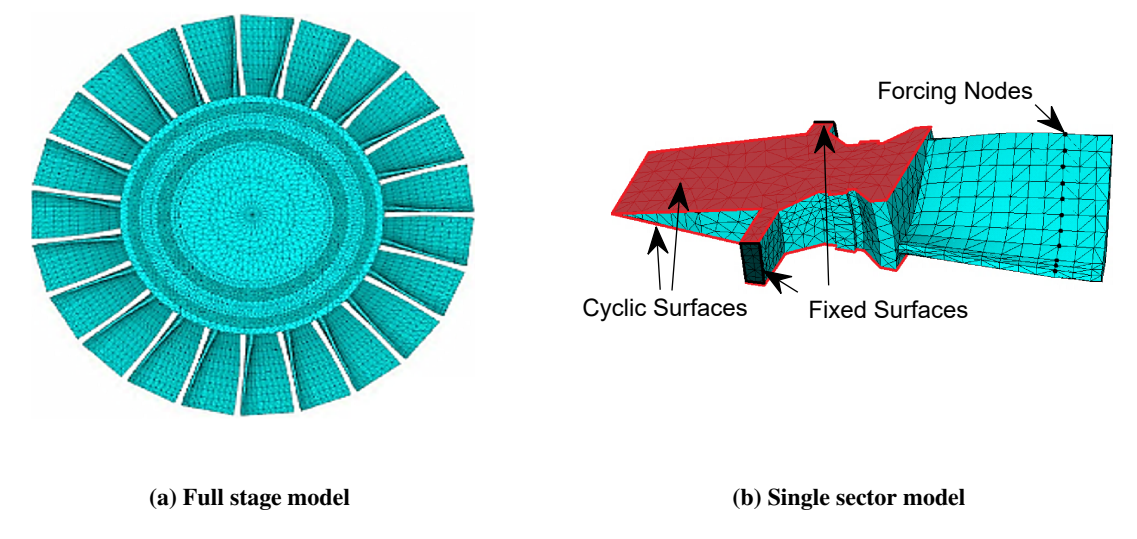


Fig. 6 Sample bladed disk finite element model

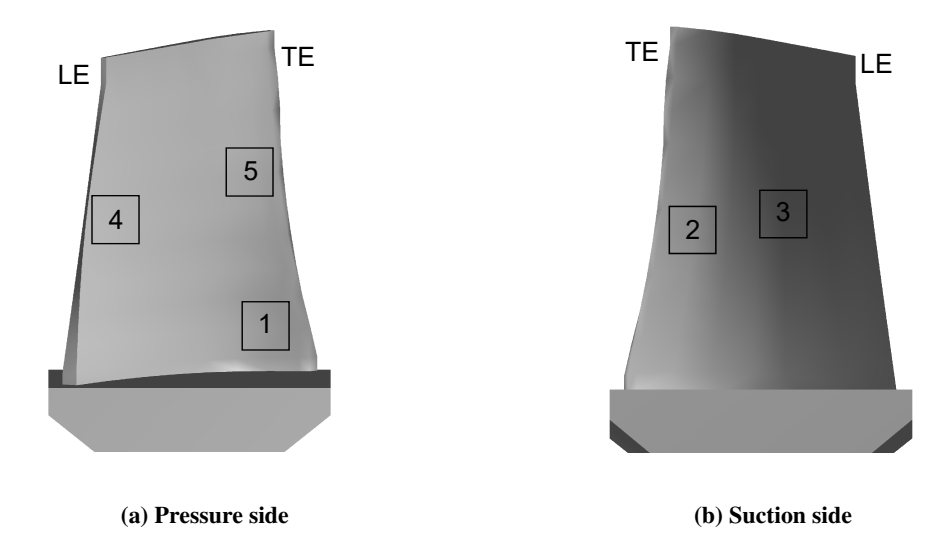


Fig. 7 Approximate strain gauge locations on blade

#### **PROM**

PROMs have been developed to allow quick changes to various parameters within the reduced space, such as rotational speed effects. A procedure to create a ROM for a system rotating at a desired rotational speed including mistuning was previously published [22]. This method requires three modal analyses at evenly spaced speeds carried out in the reduced space to form a ROM that includes the prestress effects at any desired speed. A change in rotational speed has been shown to shift the stiffness of bladed disks due to a combination of stress stiffening and spin-softening effects.

In order to parameterize the variation in rotational speed, a method by Hong et al. [29] was utilized. The goal of this process is to estimate the stiffness at a desired speed p using a quadratic interpolation, which can accurately model both the effects of spin-softening and stress stiffening. The quadratic interpolation of the stiffness matrix can be seen in Eq. (2). Note that the  $\frac{\partial \mathbf{K}}{\partial p}$  and  $\frac{\partial^2 \mathbf{K}}{\partial p^2}$  values in the equation cannot be calculated directly, and are approximated using forward difference quantities. The first, lowest rotational speed for this work is represented as  $p_0$ .

$$\mathbf{K}(p) = \mathbf{K}(p_0) + \frac{\partial \mathbf{K}}{\partial p}(p - p_0) + \frac{1}{2} \frac{\partial^2 \mathbf{K}}{\partial p^2}(p - p_0)^2$$
 (2)

While a quadratic interpolation can be used to estimate the stiffness at a new target speed, the goal is to apply this new approximation in the reduced space to reduce computational costs. A selection of tuned mode shapes,  $\Phi$ , can be used to reduce the mass,  $\mathbf{M}$ , and stiffness,  $\mathbf{K}$ , matrices. To create a valid transformation, the system modes are calculated for all three rotational speeds and combined to create an augmented reduction matrix,  $\Phi_{aug}$ . To create an orthogonal, well-conditioned basis, a singular value decomposition is performed, and the appropriate left singular vectors are selected. These singular vectors are grouped in a transformation matrix  $\mathbf{U}$ . This  $\mathbf{U}$  matrix is then used to

reduce the M and K matrices. The resulting, reduced stiffness matrix, taking into account all three rotational speeds, is given in Eq. (3).

$$\mathbf{K}_{PROM}(p) = \mathbf{U}^{T} \mathbf{K}_{FD}^{0} \mathbf{U} + \mathbf{U}^{T} \mathbf{K}_{FD}^{1} \mathbf{U}(p - p_{0}) + \frac{1}{2} \mathbf{U}^{T} \mathbf{K}_{FD}^{2} \mathbf{U}(p - p_{0})^{2}$$
(3)

The mass matrix does not change with rotational speed, so the mass matrix from any of the speeds can be utilized. The resulting, reduced mass matrix is given in Eq. (4).

$$\mathbf{M}_{PROM} = \mathbf{U}^T \mathbf{M}(p_0) \mathbf{U} \tag{4}$$

These PROMs were generated for both the freestanding and damped cases, where for each case three prestressed modal analyses were used to construct each PROM. This method gives the best results when the desired rotational speed is within the bounds of the three solved rotational speeds, so it is typically best to conduct the analysis over a wide operational range from 0 RPM to the maximum desired operating speed. The resulting PROM models a bladed disk with no mistuning present. The next section describes the incorporation of small frequency mistuning modeling into the PROM.

#### **PROM** with Small Mistuning

In order to apply small mistuning to the system, the CMM method by Lim et al. [30] was chosen to be implemented. Small mistuning is modeled as stiffness deviations in the blades. This will break the cyclic symmetry of the system and will result in a more complex behavior of the individual blade mode shapes and frequencies. In this work, small shifts in the blade-to-blade frequencies were modeled by changing the modulus of elasticity of each blade appropriately. These changes can be used to generate a delta stiffness matrix,  $\mathbf{K}_{\delta}(p)$ , that was added to the tuned system stiffness matrix defined in the PROM section. The mass matrix remains the same since only frequency mistuning is considered in this work.

To calculate the mistuned eigenvalue deviation, the cantilever blade modes, along with the tuned normal modes, are used to calculate the participation factors used in the CMM method. These are used to project the mistuning on the full system. This process uses the mistuning pattern  $\mathbf{m}_j(p)$ , the cantilever blade eigenvalues  $\mathbf{\Lambda}^{CB}$ , and the tuned cantilever blade modes  $\mathbf{\Phi}^{CB}(p)$ . These values are summed over the total number of blades, N. This summation can be seen below in Eq. (5).

$$\mathbf{K}_{\delta}(p) = \sum_{j=1}^{N} \mathbf{q}_{j}^{T}(p) \mathbf{m}_{j}(p) \mathbf{\Lambda}^{CB} \mathbf{q}_{j}(p)$$
(5)

This summation, when used with a PROM, must be done for three rotational speeds. The cantilever blade stiffness  $\mathbf{K}^{CB}$ , cantilever blade eigenvalues  $\mathbf{\Lambda}^{CB}$ , and cantilever blade modes  $\mathbf{\Phi}^{CB}$  are found using a modal analysis on one sector of the model, where the disk degrees of freedom are held fixed. This method is valid for the freestanding case, but for the two damper cases, modeling the cantilever blades is more complicated. The method for the stuck and sliding damper cases will be expanded upon in the Damper Modeling section of this report. As with the PROM, these values are extracted for all three evenly spaced rotational speeds. The transformation matrix  $\mathbf{U}^{CB}$  is formed in the same manner as  $\mathbf{U}$  for the pristine PROM using a singular value decomposition.  $\mathbf{U}^{CB}$  represents the full transformation matrix for the cantilever blade system. To obtain the diagonal eigenvalue matrix at a desired speed,  $\mathbf{\Lambda}^{CB}(p)$ , a quadratic interpolation must again be used. After the transformation and stiffness matrices are calculated, the participation factors at a desired speed,  $\mathbf{q}_{I}(p)$ , can be determined for each sector. The equation for calculating the participation factors,  $\mathbf{q}_{I}(p)$ , can be seen below in Eq. (6). The values  $\mathbf{K}_{FD}^{CB,0}$ ,  $\mathbf{K}_{FD}^{CB,1}$ , and  $\mathbf{K}_{FD}^{CB,2}$  follow the same procedure as described in the PROM method section.

$$\mathbf{q}_{j}(p) = \mathbf{\Lambda}^{CB}(p)^{-1} [\mathbf{U}^{CB^{T}} \mathbf{K}_{FD}^{CB,0} \mathbf{U}_{CBj} + \mathbf{U}^{CB^{T}} \mathbf{K}_{FD}^{CB,1} \mathbf{U}_{CBj}(p - p_{0}) + \frac{1}{2} \mathbf{U}^{CB^{T}} \mathbf{K}_{FD}^{CB,2} \mathbf{U}_{CBj}(p - p_{0})^{2}]$$
(6)

Lastly, the mistuning values,  $\mathbf{m}_j$ , need to be determined. The mistuning parameters can be quadratically interpolated in the same manner as the other values as shown in Eq. (7), with a key difference being that the mistuning values trend toward zero as rotational speed increases.

$$\mathbf{m}_{j,p_o} = \mathbf{m}_{j,p_oP} + \mathbf{m}_{j,p_o+\Delta P}(p - p_0) + \frac{1}{2} \mathbf{m}_{j,p_o+\Delta P}(p - p_0)^2$$

$$(7)$$

With  $\mathbf{K}_{\delta}(p)$  in Eq. (5) defined, the PROM stiffness matrix, including small mistuning, can be defined. This stiffness matrix definition can be seen in Eq. (8).

$$\mathbf{K}_{PROM} = \mathbf{U}^T \mathbf{K}(p) \mathbf{U} + \mathbf{K}_{\delta}(p)$$
 (8)

The value for the mass matrix,  $\mathbf{M}_{PROM}$ , is unchanged. The  $\mathbf{M}_{PROM}$  and  $\mathbf{K}_{PROM}$  now model the system at a specified rotational speed while taking into account small stiffness mistuning.

#### **Damper Modeling**

Adding damping elements, such as under-platform dampers, to the bladed disk makes creating an efficient computational modeling tool much more challenging than the freestanding case. This difficulty arises due to friction damping adding a nonlinearity into the system. The mode shapes and natural frequencies are no longer independent of the applied forcing, this is due mainly to the state of the damper (i.e., stuck, microslip, macroslip) changing based on the excitation conditions. The full dynamics of the nonlinear system are quite difficult to capture effectively for a full or a reduced order model. Instead, in this work two linear ROMs were created that are extreme cases of the nonlinear system (i.e., the fully stuck damper state and the fully sliding damper condition with no friction). The CMM method was adjusted slightly to accommodate the addition of the damper. The goal in creating these linear ROMs with the damper is to create reasonable bounds for the measured nonlinear response.

It should be noted that the two linear models are limited in how they can capture the exact trend of frequency and amplitude versus forcing, but more so capture the bounds of the resonant frequencies of the nonlinear system, and do not ensure that they will bound the amplitude of the response. These linear models provide these bounds for the system since it is weakly nonlinear.

The CMM method can be applied for both the stuck and sliding cases, but instead of being able to solve the single sector cantilever blade mode, the damper must be modeled using a cyclic symmetry analysis similar to the normal modes. The cyclic symmetry allows the damper to move as it would for the normal modes. This movement of the damper in turn changes the mode shapes of the system. The disk nodes will again be held fixed when solving for the cantilever blade modes. CMM assumes that the cantilever blade mode shapes can be used to approximate the normal mode shapes of the blades from the full system. Therefore, the damper must be modeled in the same way as it was for the normal modes. This ensures that the damper is in the same location between the cantilever blade analyses and full system modal analyses.

#### **Rotational Forcing Method**

In order to compare the computational ROM results to the physical test data, a tip deflection must be calculated with the reduced matrices found from the CMM-PROM method. These tip deflections will be obtained by using a time integration method that will simulate the testing conditions. The reduced values allow for equations of motion to be solved in a reasonably short amount of time. This time integration is able to show transient behavior that a traditional harmonic analysis is not able to capture. A traditional harmonic analysis is only able to capture stationary periodic steady state motions that do not include the transient behavior of the differential equations of motion. The reduced equations of motion, that will be solved using a rotational forcing, is defined in Eq. (9). This rotational forcing is modeled using a force sweeping across a row of singular blade nodes of the FE model. This should give a valid approximation for the forcing seen by the blade during the testing. It is important to note that the forcing applied in

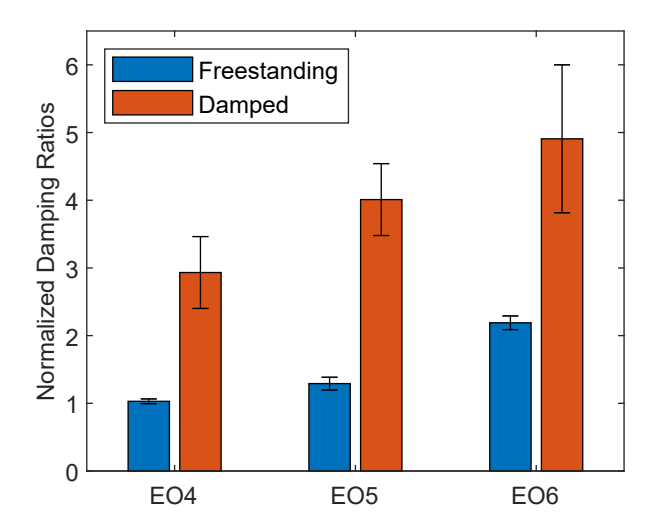


Fig. 8 Damping ratios for different engine orders for damped and undamped blades

the experiments and computational models are much simpler than that seen in a real-world gas turbine. An expanded explanation for the rotational forcing time integration can be seen in the work by Kurstak and D'Souza [20].

$$\mathbf{M}_{PROM}\ddot{x} + \mathbf{C}_{PROM}\dot{x} + \mathbf{K}_{PROM}x = \mathbf{F}_{Applied}(t)$$
(9)

Proportional (Rayleigh) damping is used to model the  $C_{PROM}$  matrix. The equation for proportional damping can be seen in Eq. (10). The mass  $(\alpha)$  and stiffness  $(\beta)$  multipliers terms can be calculated from the modal damping ratio  $\zeta_i$  at a particular natural circular frequency  $\omega_i$  using  $\zeta_i = \frac{\alpha}{2\omega_i} + \frac{\beta\omega_i}{2}$ . For the ROM in this study,  $\alpha$  is neglected  $(\alpha=0)$ , so the proportional damping term for the first bending mode is simplified to  $\beta = \frac{2\zeta}{\omega_{ave}}$ .  $\omega_{ave}$  represents the average natural frequency for all the blades in each run. The damping ratios,  $\zeta$ , were determined from the experimental runs and are also an average over all the blades for each run. These damping ratios are valid over the first bending mode frequency range. The damping values were extracted using the half-power bandwidth method at the resonance peak. The normalized damping ratios for the different engine orders are shown in Fig. 8. Note that the damping increases with increasing engine orders for both the freestanding and the damped cases. This is expected because the increase in rotational speed at lower engine orders will have higher radial loads due to the centrifugal force that will result in less movement at the blade-disk interface, resulting in less damping. This trend has been previously shown and discussed in [19].

$$\mathbf{C}_{PROM} = \alpha \mathbf{M}_{PROM} + \beta \mathbf{K}_{PROM} \tag{10}$$

Forcing amplitudes were chosen to match the average experimental blade deflections for each run. The forcing amplitude is tuned to match the results for the x1 forcing case and then linearly increased to model the higher forcing cases. These forcing magnitudes will be different for the freestanding and damped cases. The forcing was also applied to

the blades in the PROM in roughly the same location as the blades were forced during the experiment. It is important to note that the equation is solved in the reduced space, so to produce tip deflections the results must be transformed back into the physical space. This time integration is relatively fast and allows for many models to be run simultaneously.

#### IV. Results and Validation

In this section, the computational ROMs are validated using the experimental strain gauge and tip timing data. It is important that the operating conditions (i.e., rotational speed) and forcing conditions (i.e., EO and forcing magnitude) are matched between the experiments and computational simulations. Rotational speeds, accelerations, active jet count (EO), and forcing pressure for the ROM are also selected to match the experimental runs. The experiments and the results of this report are focused on EO 4, 5, and 6. As discussed, four blades were wired with extra strain gauges, but only one blade was chosen that gave the best match of the strain distribution of the full order FE model with the experiments for this work to provide a concise presentation of the results.

The three, evenly spaced rotational speeds chosen to build the PROM were 0 RPM, 7,500 RPM, and 15,000 RPM. The individual blade to blade stiffness mistuning values and average damping ratio were determined using the Agilis Tip Timing software. These mistuning values can be directly inserted into the CMM-PROM method as previously discussed. The average damping ratio was used to find the  $\beta$  value as discussed in the previous section. Comparisons between the computational models and experiments will be made over a number of the rotating forcing amplitudes to verify the validity of the PROMs in capturing the underlying system dynamics. The dynamics that are the most important to capture are the amplitudes and response frequencies of the blades. The results of the PROM are time integrated with an EO 4, 5, or 6 forcing that sweeps over the blade nodes of the model as discussed in the previous section. This mimics the experiments and gives an accurate representation of the blade tip deflections.

The reduced matrices are roughly 0.0125% the size of the original matrices extracted from the FE model. The new matrix is reduced to approximately 250 degrees of freedom. To emphasize the effectiveness of the ROM method, relative errors were found between natural frequencies of the ROM and the full FE model at the same rotational speed. The frequency errors that were found were well under 0.1%, which is consistent with errors published in previous literature[22].

Due to the proprietary nature of some of the work all forcing levels, forcing frequencies, and deflection values will be nondimensionalized against baselines of each run. Tip deflections for the freestanding case are force-normalized since the system is linear. The blade tip deflections for the damper case, due to the nonlinearity, will not be force normalized, but will be scaled with respect to the maximum deflection per case and therefore cannot be compared from case to case in this work. The forcing frequency will be normalized to the percentage of each test run. Both the freestanding and damped cases will be discussed in the following sections.

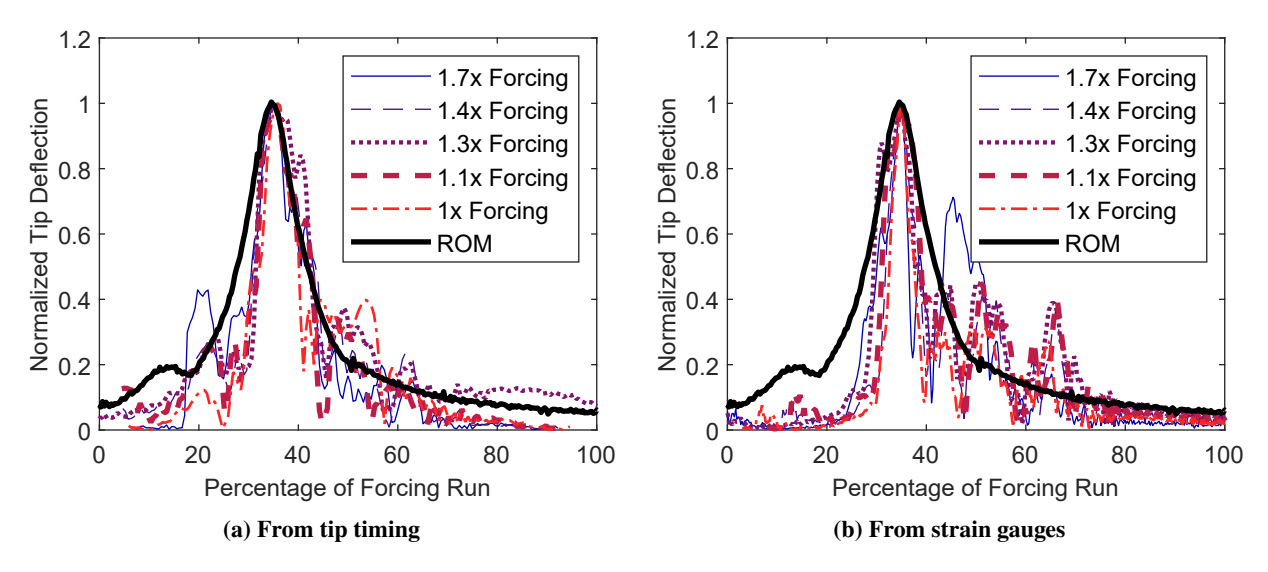


Fig. 9 EO 6 freestanding normalized tip deflections

#### **Freestanding Results**

First, the freestanding data for the strain gauges and tip timing will be analyzed to validate the CMM-PROM method. The normalized excitation levels that will be focused on for the freestanding cases are from 1 to 1.7 times the base forcing. The normalized tip deflections for the freestanding bladed disk, for each of the forcing magnitudes of EO 6, 5, and 4 can be seen in Fig. 9, Fig. 10, and Fig. 11, respectively. The plot on the left, for each of the EOs, is the tip timing measurement and the plot on the right is the tip deflections extracted from strain gauge data, and the thick solid line is the computational ROM results.

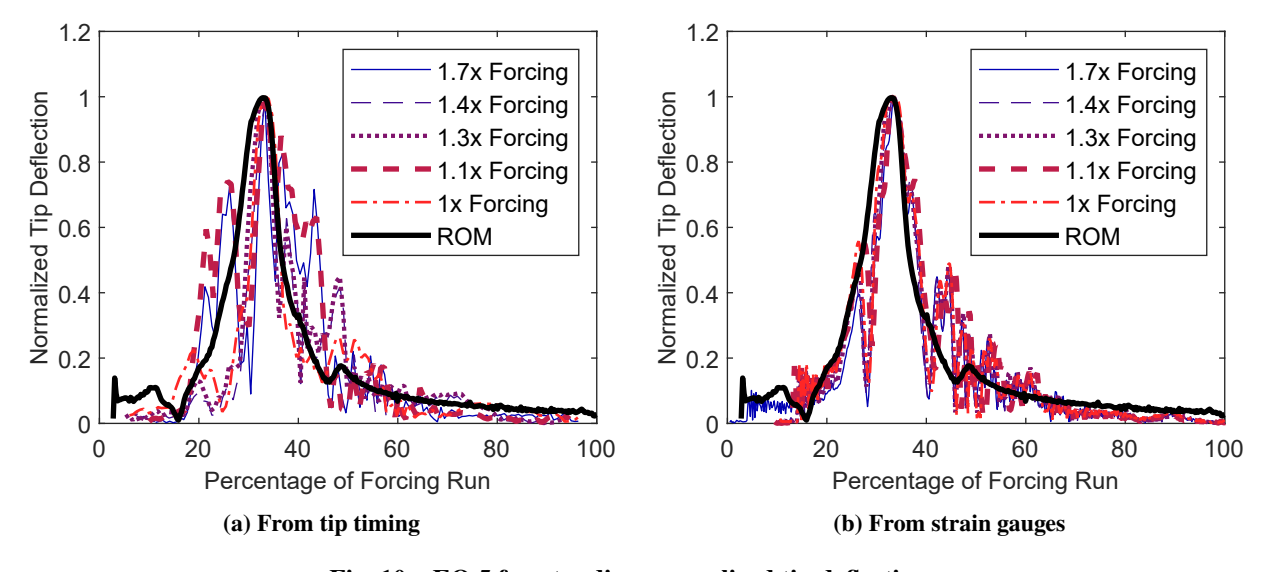


Fig. 10 EO 5 freestanding normalized tip deflections

In reviewing the plots, it is clear that the computational ROM does an excellent job of matching both the amplitude and the main frequency response from the experiments for all three EO excitations. Moreover, the light probes and

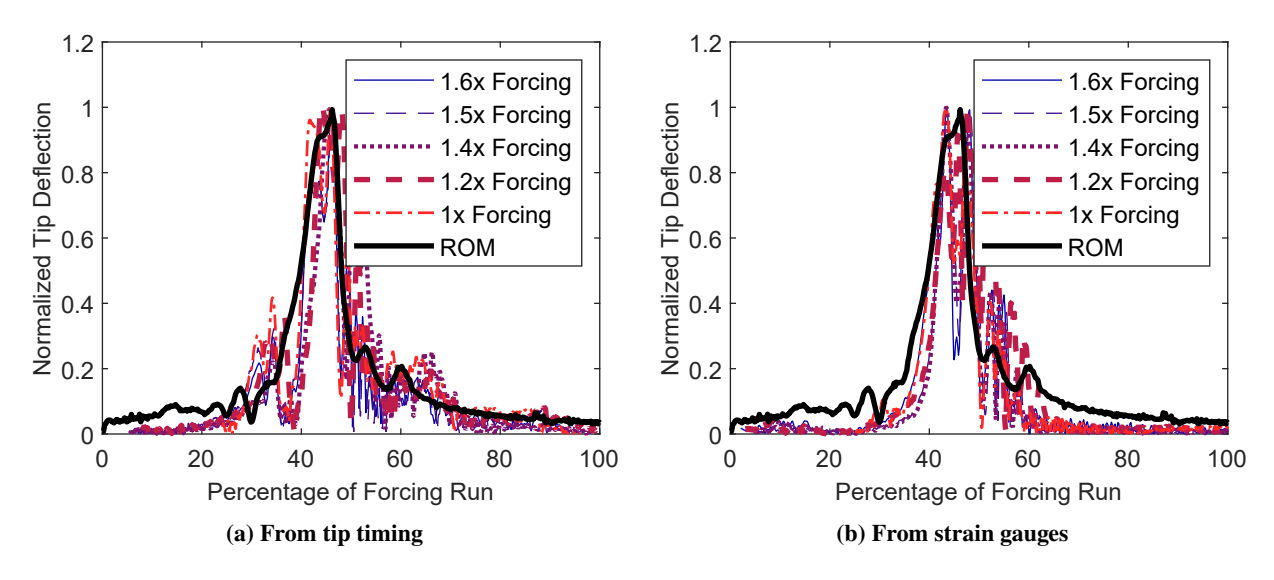


Fig. 11 EO 4 freestanding normalized tip deflections

the strain gauge measurements are also in very good agreement. Since the freestanding case is a linear system at a given rotational speed, the different levels of forcing should all match up well. While the amplitudes tend to match up quite well at the main peak (where they agree very well with the computational results), there tends to be more uncertainty and variation away from this peak. This is to be expected since at the peak there is the strongest response of the system to the excitation signal, other sources of noise or perturbations will have a larger affect away from this resonance peak. Although the computational model captures the main peak accurately, it does not capture all of the off-peak responses. There are a number of reasons why these are not captured in the computational model, including: the boundary conditions of the model, which has the bladed disk but not the shaft, bearing system and test stand; the back pressure in the tank that rises over the course of the experiment as the air jets excite the bladed disk; and any excitation and measurement noise in the experiments that are not captured in the computational model.

It should also be noted that, while there is a very good agreement at the main peak between the tip timing and strain gauges, away from the peak there is again more variation. Some of this can be explained by the fact that the strain gauge response is being related to the tip timing results through the ROM, which does exclude a number of components including the shaft, bearing system and stand. It should also be noted that the strain gauge data is more reliable and repeatable across different forcing amplitudes, which is evident in the plots, particularly for EO 5 and 6. This is likely due to the much higher sampling frequency of the strain gauge measurements. The actual amplitude of the response for each EO was different with EO 6 having the highest response and EO4 the lowest. This is not evident in the plots since they have all been normalized to one, however this is expected since there are more excitation points per revolution at higher EO values. Moreover, as seen in Fig. 3 the bladed disk is less stiff at higher EO values since the rotating speed is lower.

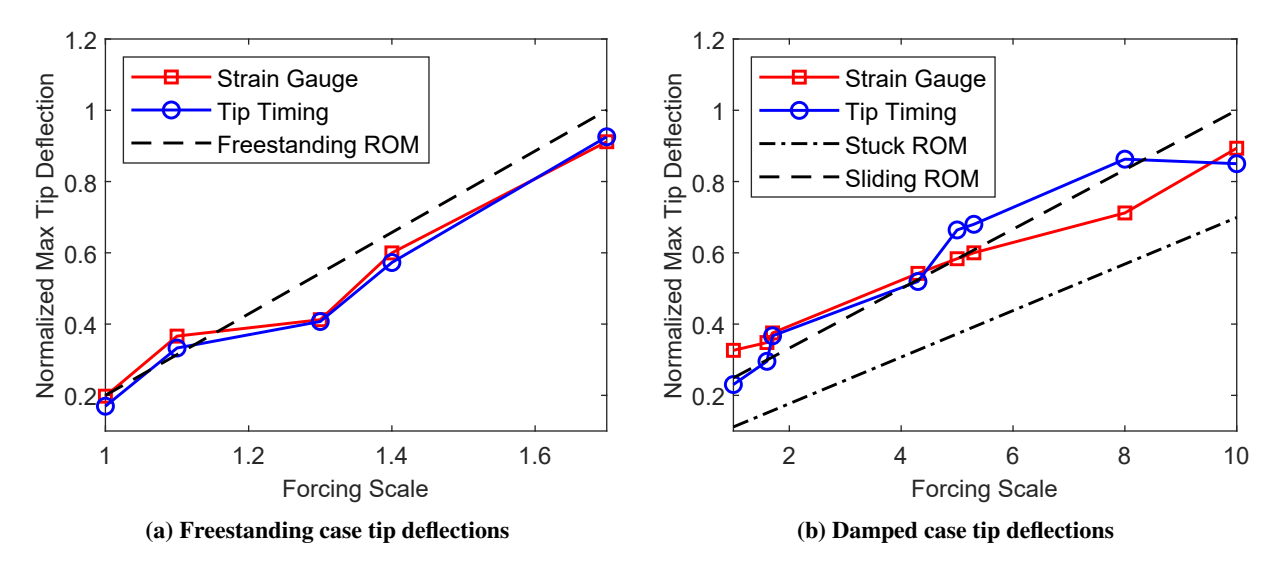


Fig. 12 Forcing magnitude versus tip deflection for EO 6 freestanding and damped cases

#### **Damped Results**

Next, the damped cases will be analyzed to show that the two linear damper models can be used to determine the bounds of the measured data of the nonlinear system. Note that the two linear cases are when the damper is allowed to slide without friction and when the damper is completely stuck to the blade. Because the dampers were able to effectively decrease the amount of tip deflection, the forcing magnitudes were able to be much larger than the freestanding case without high cycle fatigue concerns. The forcing magnitude scaling factor implemented within the damped ROMs were tuned and match that of the freestanding model reasonably well. The excitation levels that will be focused on in the damped cases are up to 12.2 time that of the base forcing. The results from a forcing amplitude and tip deflection comparison, for EO 6, can be seen in Fig. 12. This comparison is done for the response of the single blade that is the focus of this study. Similar results were found for engine orders 4 and 5 but are omitted for the sake of brevity. The freestanding case shows a strong linear relationship between forcing scale and normalized maximum tip deflection, while the damper cases are more complicated. For the two damped cases, the ROM methods give reasonable results for the amplitudes, with a significant deviation in the strain gauge and tip timing results at higher forcing levels. It should be noted that although the strain gauges were likely more reliable in the freestanding case, this is not so for the damped case. This is due to the use of the linear ROMs used to transform the strain gauge data to tip deflections, which neglect the nonlinear effects of how the mode shapes change based on the forcing amplitude and contact status of the damper. It should be noted that, for this specific bladed disk configuration, the frictionless sliding ROM gives a good representation for the amplitudes seen in the EO 6 testing.

The non-dimensionalized tip deflections for the sliding and stuck damper cases for EO 6 can be seen in Fig. 13. The results for EO 5 and EO 4 can be seen in Fig. 14 and Fig. 15, respectively. The fully stuck and frictionless sliding ROM results are pointed out using arrows in the figures. Each of the forcing amounts are scaled for the individual engine

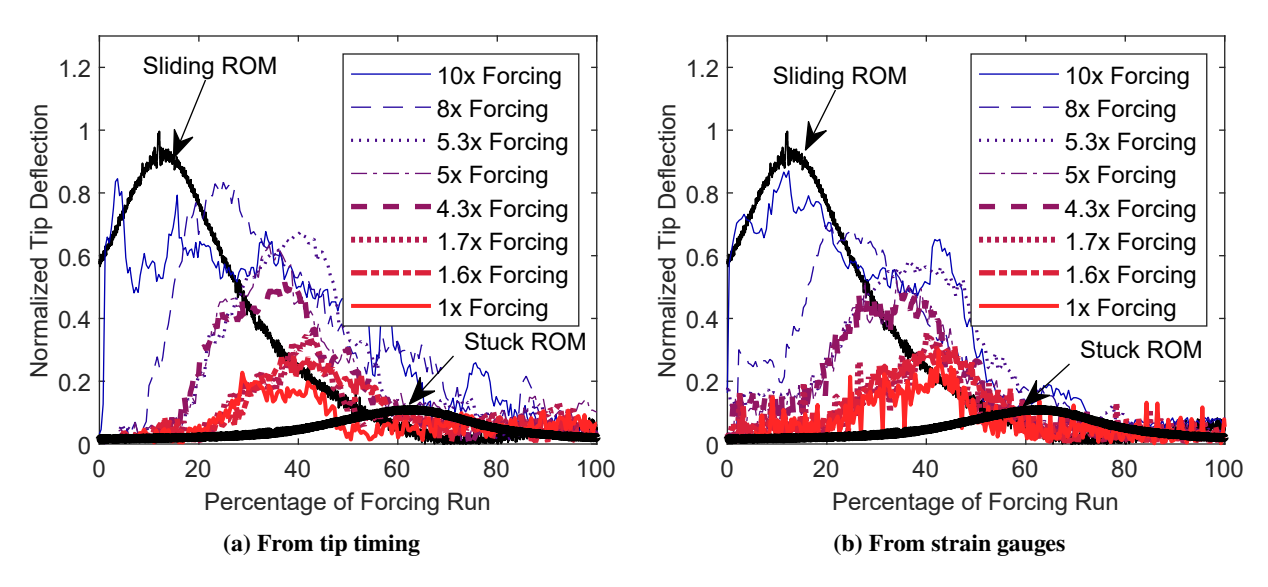


Fig. 13 EO 6 damped normalized tip deflections

order figures, so x1 forcing between EOs are not necessarily the same magnitude.

Note that in contrast to Figs. 9-11, the response amplitudes have not been normalized by the forcing magnitude since the system is nonlinear. The sliding ROM plotted corresponds to the maximum forcing (10x for EO6, 12.2x for EO5 and 7.1x for EO 4), and the stuck ROM corresponds to the minimum forcing (1x). The linear ROMs were plotted in this manner to try and show the expected bounds in both frequency and amplitude as the forcing level increases.

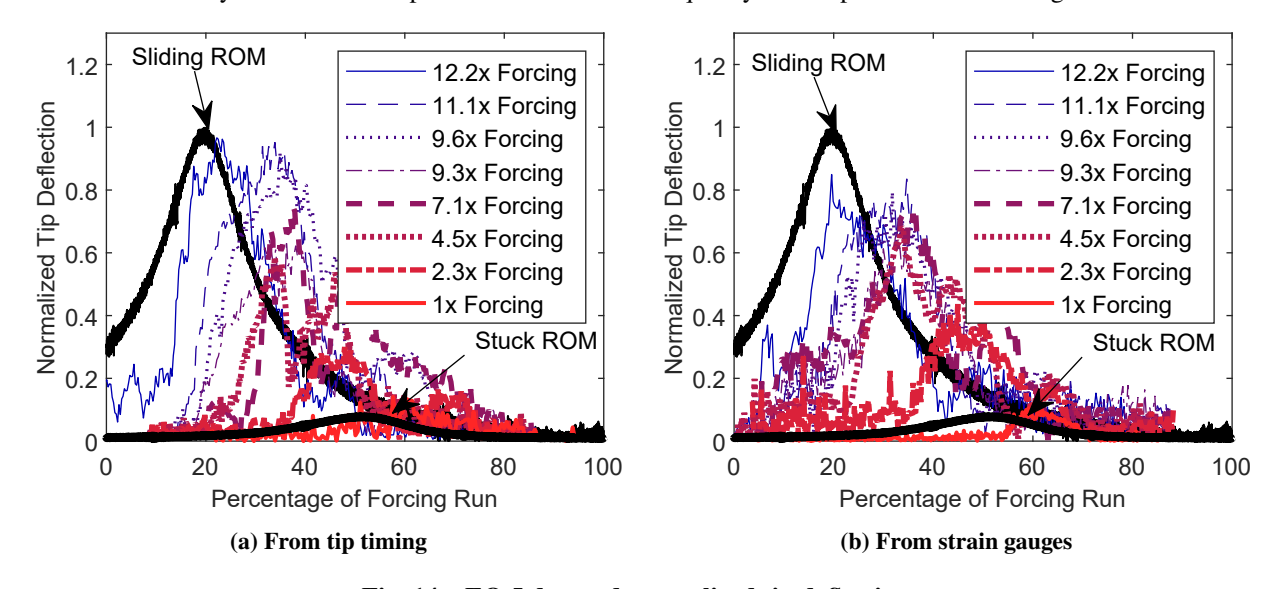


Fig. 14 EO 5 damped normalized tip deflections

Focusing first on Fig. 13 and Fig. 14, it is clear that the linear ROMs provide a good bound for the response. It is clear that the stuck ROM is an upper bound for the resonant frequency of the damped system, which corresponds to the case where the excitation is very low and forcing is not large enough to cause any motion in the damper due to low response of the blades. The amplitude of the response is pretty close to the 1x forcing case as well. The sliding ROM

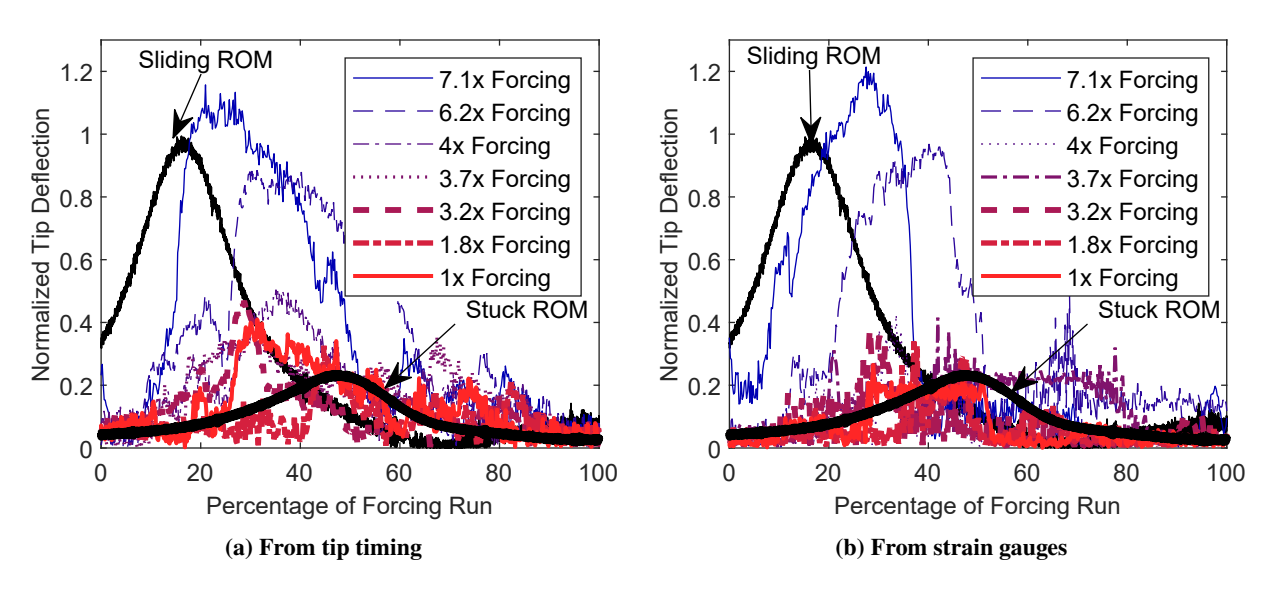


Fig. 15 EO 4 damped normalized tip deflections

captures the free translational motion of the damper without friction, which provides a lower bound for the resonance frequency. This lower bound corresponds to the case where the damper is in full macroslip (without the damping due to friction), so it rightly predicts a larger response than the highest forcing case and a lower frequency. It should also be noted that the peaks for these experimental damped cases are broader than the linear computational models. This is to be expected due to the increased damping that has the effect of flattening the peak such that it is a lower magnitude over a larger frequency range. It should also be noted that the two linear models are limited in how they can capture the exact trend of frequency and amplitude versus forcing, but more so captures the bounds of the nonlinear system for these characteristics.

Looking next at Fig. 15, some of the trends in the previous figures are observed but it is much less clear. At low excitation levels the response is really spread out and the peak is hard to establish, so the stuck ROM does not necessarily provide an upper bound on the maximum frequency. The sliding case still appears to provide a good bound on the lower frequency range, but no longer provides a good bound for the response amplitude.

#### V. Conclusions

This work discusses the modeling of full scale rotating experiments of bladed disks with and without under-platform dampers. The bladed disk dynamic responses were measured by both strain gauges and tip timing measurements. These measurements are compared using a high fidelity full order model of the bladed disk, and are shown to be in good agreement. Additionally, the full order model is reduced significantly using a parametric reduced order model and component mode mistuning so that it can capture both the rotational speed effects and small stiffness mistuning in the system. This computational model is then simulated in way that captures the underlying dynamics of the experiments and is shown to be in good agreement with the experimental data.

The freestanding model is able to capture not only the frequencies of the response, but also accurately capture the tip deflection amplitudes. The two linear damper cases investigated are able to capture the estimated bounds for the frequency of the nonlinear damper test cases. The two linear damper cases are less accurate in predicting the tip deflection amplitudes because of the nonlinearities introduced by the damper that are not captured by the linear ROMs, but the two cases give good estimates for the tip amplitudes. Overall, it can be concluded that the two linear ROMs give a good bound for the nonlinear damper system dynamics. Since not a lot of work has been done that investigates under-platform dampers in rotating rigs with representative hardware, this work is important in providing insight into how these experiments can be efficiently modeled.

Future directions of this work include implementing additional nonlinear behaviors into these models to try and capture the exact characteristics seen in the experiments. As discussed, the linear models do not take into account the dissipation due to friction and other complex nonlinear states (i.e., loss of contact). The current linear models were used to find the bounds of the system and not to perfectly match the physical system. This is a key limitation of the current work that needs to be addressed in future work. Another improvement to this work is the inclusion of small geometric mistuning in the blades which has been shown in previous studies to be an effective method for modeling freestanding bladed disks. Some other future work may include adding the shaft, shaft coupling, and other hardware components that were not included in the presented work. An extended model could also be used for the comparison between the strain gauge and tip timing data and in investigating how the strain values can be more accurately converted to tip deflections.

# VI. Acknowledgments

The authors would like to acknowledge the financial support of Siemens Energy Inc. in running the experiments and the support of program manager Heinrich Stueer. Additionally, the analysis was supported by the US National Science Foundation under Grant No. 1902408, program manager Dr. Harry Dankowicz. The authors gratefully acknowledge the support of the OSU GTL staff members and Dr. Randall Mathison in the setup and operation of the facility. The authors would also like to acknowledge Agilis Measurement Systems and their chief scientist, Ron Washburn, for their help in providing advice and technical support for the Agilis c360 software and blade tip timing system. Any opinions, findings, and conclusions or recommendations expressed in this paper are those of the authors and do not necessarily reflect the views of the National Science Foundation or Siemens Energy Inc.

#### References

- [1] Feiner, D. M., and Griffin, J. H., "Mistuning Identification of Bladed Disks Using a Fundamental Mistuning Model–Part I: Theory," *Journal of Turbomachinery*, Vol. 126, No. 1, 2004, pp. 150–158. https://doi.org/10.1115/1.1643913, URL http://dx.doi.org/10.1115/1.1643913.
- [2] Bladh, R., Castanier, M. P., and Pierre, C., "Component-Mode-Based Reduced Order Modeling Techniques for Mistuned

- Bladed Disks Part I: Theoretical Models," *Journal of Engineering for Gas Turbines and Power Transactions of the ASME*, Vol. 123, No. 1, 2001, pp. 89–99. https://doi.org/10.1115/1.1338947.
- [3] Bladh, R., Castanier, M. P., and Pierre, C., "Component-Mode-Based Reduced Order Modeling Techniques for Mistuned Bladed Disks Part II: Application," *Journal of Engineering for Gas Turbines and Power Transactions of the ASME*, Vol. 123, 2001, pp. 100–108.
- [4] Baek, S., Zhao, Y., and Epureanu, B. I., "Reduced Order Models of Blisks With Small Geometric Mistuning," *Proceedings of the ASME Turbo Expo 2016: Turbomachinery Technical Conference and Exposition*, ASME, Seoul, South Korea, 2016, pp. 1–10. https://doi.org/10.1115/GT2016-57829.
- [5] Beck, J. A., Brown, J. M., Runyon, B., and Scott-Emuakpor, O. E., "Probabilistic Study of Integrally Bladed Rotor Blends using Geometric Mistuning Models," AIAA SciTech Forum, American Institute of Aeronautics and Astronautics, 2017. https://doi.org/10.2514/6.2017-0860.
- [6] Beck, J. A., Brown, J. M., Kaszynski, A. A., Carper, E. B., and Gillaugh, D. L., "Geometric Mistuning Reduced-Order Model Development Utilizing Bayesian Surrogate Models for Component Mode Calculations," *Journal of Engineering for Gas Turbines and Power*, Vol. 141, No. 10, 2019. https://doi.org/10.1115/1.4044454, URL https://doi.org/10.1115/1.4044454, 101013.
- [7] Madden A.; Epureanu, S., B. I.; Filippi, "Reduced-Order Modeling Approach for Blisks with Large Mass, Stiffness, and Geometric Mistuning," AIAA Journal, Vol. 50, No. 2, 2012, pp. 366–74. https://doi.org/10.2514/1.j051140, URL http://arc.aiaa.org/doi/pdf/10.2514/1.J051140.
- [8] D'Souza, K., and Epureanu, B. I., "A Statistical Characterization of the Effects of Mistuning in Multistage Bladed Disks," *Journal of Engineering for Gas Turbines and Power*, Vol. 134, No. 1, 2011, pp. 1–8. https://doi.org/10.1115/1.4004153, URL http://link.aip.org/link/?GTP/134/012503.
- [9] Besem, F. M., Kielb, R. E., Galpin, P., Zori, L., and Key, N. L., "Mistuned Forced Response Predictions of an Embedded Rotor in a Multistage Compressor," *Journal of Turbomachinery*, Vol. 138, No. 6, 2016. https://doi.org/{10.1115/1.4032164}.
- [10] Kurstak, E., and D'Souza, K. X., "Multistage Blisk and Large Mistuning Modeling using Fourier Constraint Modes and PRIME," *Journal of Engineering for Gas Turbines and Power*, 2017. https://doi.org/10.1115/1.4038613, URL http://dx.doi.org/10.1115/1.4038613.
- [11] Kurstak, E., and D'Souza, K., "Parametric Reduced Order Models for Bladed Disks With Mistuning and Varying Operational Speed," *J. Eng. Gas Turbines Power*, Vol. 142, No. 4, 2019. https://doi.org/10.1115/1.4045023, 041015.
- [12] D'Souza, K., Jung, C., and Epureanu, B. I., "Analyzing Mistuned Multi-Stage Turbomachinery Rotors with Aerodynamic Effects," *Journal of Fluids and Structures*, Vol. 42, 2013, pp. 388–400. https://doi.org/10.1016/j.jfluidstructs.2013.07.007.

- [13] Pourkiaee, S., and Zucca, S., "A Reduced Order Model for Nonlinear Dynamics of Mistuned Bladed Disks With Shroud Friction Contacts," *Journal of Engineering for Gas Turbines and Power*, Vol. 141, No. 1, 2019.
- [14] Pesaresi, L., Salles, L., Jones, A., Green, J., and Schwingshackl, C., "Modelling the nonlinear behaviour of an underplatform damper test rig for turbine applications," *Mechanical Systems and Signal Processing*, Vol. 85, 2017, pp. 662 – 679. https://doi. org/https://doi.org/10.1016/j.ymssp.2016.09.007, URL http://www.sciencedirect.com/science/article/pii/S0888327016303466.
- [15] Laxalde, D., Thouverez, F., Sinou, J. J., and Lombard, J. P., "Qualitative Analysis of Forced Response of Blisks with Friction Ring Dampers," *European Journal of Mechanics A/Solids*, Vol. 26, No. 4, 2007, pp. 676–687.
- [16] Laxalde, D., and Thouverez, F., "Non-Linear Vibrations of Multi-Stage Bladed Disks Systems with Friction Ring Dampers," Proceedings of the ASME International Design Engineering Technical Conferences and Computers and Information in Engineering Conference 2007, Paper DETC2007-34473, ASME, Las Vegas, Nevada, USA, 2007.
- [17] Tien, M.-H., Hu, T., and D'Souza, K., "Generalized Bilinear Amplitude Approximation and X-Xr for Modeling Cyclically Symmetric Structures With Cracks," *J. Vib. Acoust*, Vol. 140, 2018, pp. 041012–10. https://doi.org/10.1115/1.4039296.
- [18] Tien, M., Hu, T., and D'Souza, K., "Statistical Analysis of the Nonlinear Response of Bladed Disks with Mistuning and Cracks," *AIAA Jounal*, Vol. 57, No. 11, 2019. https://doi.org/10.2514/1.J058190.
- [19] D'Souza, K., Kurstak, E., Ruff, K., and Dunn, M. G., "A New Experimental Facility for Characterizing Bladed Disk Dynamics at Design Speed," *AIAA Journal*, Vol. 58, No. 6, 2020. https://doi.org/10.2514/1.J058682, URL https://doi.org/10.2514/1.J058682.
- [20] Kurstak, E., and D'Souza, K., "Experimental Investigation of Bladed Disk Dynamics at Design Speed Under Synchronous Vibration," AIAA Journal, Vol. 59(10), 2021, pp. 4123–4133. https://doi.org/10.2514/1.J059827.
- [21] Kurstak, E., and D'Souza, K., "An Experimental and Computational Investigation of a Pulsed Air-Jet Excitation System on a Rotating Bladed Disk," *Journal of Engineering for Gas Turbines and Power*, Vol. 143, No. 1, 2021. https://doi.org/10.1115/1. 4049014.
- [22] Kurstak, E., Wilber, R., and D'Souza, K., "Parametric Reduced Order Models for Bladed Disks With Mistuning and Varying Operational Speed," *Journal of Engineering for Gas Turbines and Power*, Vol. 141, No. 5, 2019. https://doi.org/10.1115/1. 4041204, URL https://doi.org/10.1115/1.4041204, 051018.
- [23] Jamia, N., Friswell, M. I., El-Borgi, S., and Rajendran, P., "Modelling and experimental validation of active and passive eddy current sensors for blade tip timing," *Sensors and Actuators A: Physical*, Vol. 285, 2019, pp. 98 110. https://doi.org/https://doi.org/10.1016/j.sna.2018.10.034, URL http://www.sciencedirect.com/science/article/pii/S0924424718309701.
- [24] Zhang, J., Duan, F., Niu, G., Jiang, J., and Li, J., "A Blade Tip Timing Method Based on a Microwave Sensor," *Sensors (Basel, Switzerland)*, Vol. 17, No. 28492469, 2017, p. 1097. URL https://www.ncbi.nlm.nih.gov/pmc/articles/PMC5470487/.

- [25] Heath, S., and Imregun, M., "A Survey of Blade Tip-Timing Measurement Techniques for Turbomachinery Vibration," *Journal of Engineering for Gas Turbines and Power*, Vol. 120, No. 4, 1998, pp. 784–791. https://doi.org/10.1115/1.2818468, URL http://dx.doi.org/10.1115/1.2818468.
- [26] Battiato, G., Firrone, C., and Berruti, T., "Forced response of rotating bladed disks: Blade Tip-Timing measurements," *Mechanical Systems and Signal Processing*, Vol. 85, 2017, pp. 912–926. https://doi.org/doi.org/10.1016/j.ymssp.2016.09.019,.
- [27] Fan, Z., Li, H., Dong, J., Wei, D., Cao, H., and Chen, Y., "An improved mistuning identification and dynamic strain prediction method for rotating blades with application of blade tip timing technology," *Mechanical Systems and Signal Processing*, Vol. 184, 2022, p. 109684. https://doi.org/doi.org/10.1016/j.ymssp.2022.109684.
- [28] Chen, K., Wang, W., Zhang, X., and Zhang, Y., "New step to improve the accuracy of blade tip timing method without once per revolution," *Mechanical Systems and Signal Processing*, Vol. 134, 2019, p. 106321. https://doi.org/doi.org/10.1016/j.ymssp. 2019.106321.
- [29] Hong, S. K., Epureanu, B. I., Castanier, M. P., and Gorsich, D. J., "Parametric Reduced Order Models for Predicting the Vibration Response of Complex Structures with Component Damage and Uncertainties," *Journal of Sound and Vibration*, 2010. https://doi.org/10.1016/j.jsv.2010.09.022, URL https://www.sciencedirect.com/science/article/pii/S0022460X10006279.
- [30] Lim, S.-H., Bladh, R., Castanier, M. P., and Pierre, C., "Compact, Generalized Component Mode Mistuning Representation for Modeling Bladed Disk Vibration," AIAA Journal, Vol. 45, No. 9, 2007, pp. 2285–2298.